Ruling Out Multi-Order Interference in Quantum Mechanics

Urbasi Sinha *et al.*
Science **329**, 418 (2010);
DOI: 10.1126/science.1190545

This copy is for your personal, non-commercial use only.

Ruling Out Multi-Order Interference in Quantum Mechanics

Urbasi Sinha,[1]* Christophe Couteau,[1,2] Thomas Jennewein,[1]
Raymond Laflamme,[1,3] Gregor Weihs[1,4]*

Quantum mechanics and gravitation are two pillars of modern physics. Despite their success in describing the physical world around us, they seem to be incompatible theories. There are suggestions that one of these theories must be generalized to achieve unification. For example, Born's rule—one of the axioms of quantum mechanics—could be violated. Born's rule predicts that quantum interference, as shown by a double-slit diffraction experiment, occurs from pairs of paths. A generalized version of quantum mechanics might allow multipath (i.e., higher-order) interference, thus leading to a deviation from the theory. We performed a three-slit experiment with photons and bounded the magnitude of three-path interference to less than 10^{-2} of the expected two-path interference, thus ruling out third- and higher-order interference and providing a bound on the accuracy of Born's rule. Our experiment is consistent with the postulate both in semiclassical and quantum regimes.

Born's interpretation (*1*) of the wave function $\psi(\mathbf{r}, t)$ for a quantum mechanical state stipulates that the probability density to find a particle at position $\mathbf{r}$ and at time t is given by

$$P(\mathbf{r}, t) = \psi^*(\mathbf{r}, t)\psi(\mathbf{r}, t) = |\psi(\mathbf{r}, t)|^2 \quad (1)$$

A double-slit diffraction experiment is a direct consequence of this rule; the probability to detect a particle at $\mathbf{r}$ after passing through an aperture with two slits, A and B, is given by

$$
\begin{aligned}
P_{AB}(\mathbf{r}) &= |\psi_A(\mathbf{r}) + \psi_B(\mathbf{r})|^2 \\
&= |\psi_A|^2 + |\psi_B|^2 + \psi_A^*\psi_B + \psi_B^*\psi_A \\
&= P_A + P_B + I_{AB} \quad (2)
\end{aligned}
$$

where we have omitted the position argument for brevity and defined P_i to be the probability with only slit i ($i = A, B$) open. The corresponding (second-order) interference term can be defined as

$$I_{AB} := P_{AB} - (P_A + P_B) = P_{AB} - P_A - P_B \quad (3)$$

Within quantum mechanics, adding more paths (i.e., slits) does not add higher complexity. For three slits A, B, and C (Fig. 1), we find

$$P_{ABC} = P_A + P_B + P_C + I_{AB} + I_{AC} + I_{BC} \quad (4)$$

Therefore, by Born's rule and its square exponent (Eq. 1), interference always occurs in pairs of

possibilities and is defined as the deviation from the classical additivity of the probabilities of mutually exclusive events (*2*). These possibilities can be associated with any degree of freedom, such as spatial paths, energetic states, angular momentum states, etc. Even if multiple particles are involved, interference occurs in pairs of possibilities. Consequently, we define the third-order interference term I_{ABC} for a three-path configuration (mutually exclusive) as the deviation of P_{ABC} from the sum of the individual probabilities and the second-order interference terms:

$$
\begin{aligned}
I_{ABC} &:= P_{ABC} - (P_A + P_B + P_C + I_{AB} + \\
&\quad I_{BC} + I_{AC}) \\
&= P_{ABC} - P_{AB} - P_{BC} - P_{AC} + P_A + \\
&\quad P_B + P_C \quad (5)
\end{aligned}
$$

A physical system with such probability terms is three-path interference of a photon sent through a mask with three slits (Fig. 1). Note that the definitions in Eq. 3 and Eq. 5 are the first terms in an infinite hierarchy of interference terms (*2*).

The nonzero interference term I_{AB} is expected in all wave theories, including quantum mechanics (*3*, *4*). The next higher-order (i.e., three-path) interference term I_{ABC} will be zero in all wave theories, with a square-law relation between the field energy (or probability density) and field amplitude, which is the case in quantum mechanics with Born's rule. Moreover, if there is no interference at a certain level in the hierarchy, the higher-order terms must vanish as well (*2*).

Our aim is to establish experimentally whether the value of I_{ABC} is different from zero. We measure all seven probability terms of Eq. 5 plus the probability P_0 of detecting particles when all slits are closed. P_0 represents the probability of the empty set in an abstract definition, or a background signal in the experiment. The eight terms

are obtained by sending optical photons through three slits, which can be opened or closed individually (see Fig. 1 for the slit details and Fig. 2 for the setup). A double-slit experiment could be used to test Born's rule, but then one would have to measure the nonzero double-slit interference term and compare it with the theoretical prediction. This would be sensitive to experimental parameters such as slit dimensions, wavelength of incident photons, and distance between detector and slits, each with its attendant error. In contrast, we expect the three-path interference term I_{ABC} to be zero, with the advantage of being independent of many experimental parameters, thus enabling a more precise null test for Born's rule.

We measure the terms in Eq. 5 as well as P_0, which accounts for the inevitable detector noise and background signal. The measured quantity ε based on Eq. 5 is given by

$$
\begin{aligned}
\varepsilon = p_{ABC} - p_{AB} - p_{AC} - p_{BC} + p_A + p_B + \\
p_C - p_0 \quad (6)
\end{aligned}
$$

Here, $p \propto P$ of Eq. 5 and refers to the measured number of photons (or optical intensity, proportional to the photon number) in the various slit combinations. To give a scale to the size of a potential deviation from Born's rule, we define a normalized variant of ε called κ (Fig. 3),

$$\kappa \equiv \frac{\varepsilon}{\delta} \quad (7)$$

where

$$
\begin{aligned}
\delta &= |I_{AB}| + |I_{BC}| + |I_{AC}| \\
&= |p_{AB} - p_A - p_B + p_0| + |p_{BC} - p_B - p_C + \\
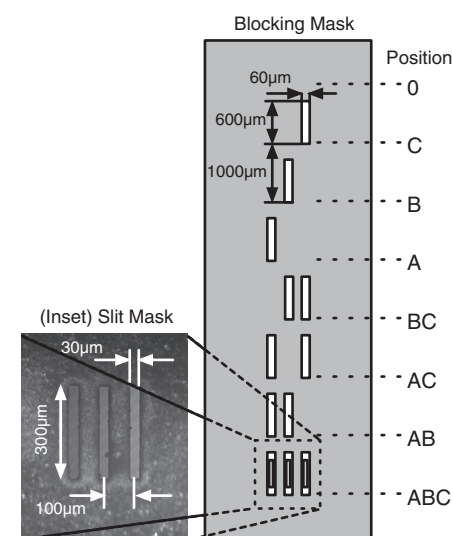&\quad p_0| + |p_{AC} - p_A - p_C + p_0| \quad (8)
\end{aligned}
$$

Fig. 1. Arrangement and dimensions of the slits used in the experiment. The blocking mask has open apertures depending on the measured slit combination according to Eq. 6. Inset is an image of the triple-slit mask.

[1]Institute for Quantum Computing and Department of Physics and Astronomy, University of Waterloo, 200 University Avenue West, Waterloo, Ontario N2L 3G1, Canada. [2]Laboratoire de Nanotechnologie et d'Instrumentation Optique, Université de Technologie de Troyes, 12 rue Marie Curie, 10 000 Troyes, France. [3]Perimeter Institute for Theoretical Physics, 31 Caroline Street North, Waterloo, Ontario N2L 2Y5, Canada. [4]Institut für Experimentalphysik, Universität Innsbruck, Technikerstraße 25, 6020 Innsbruck, Austria.

*To whom correspondence should be addressed. E-mail: usinha@iqc.ca, gregor.weihs@uibk.ac.at

Here, δ is the sum of the absolute values of the double-slit interference terms, and κ can be seen as the ratio of an unexpected three-path interference term to the expected two-path interference term. If $\delta = 0$, then $\varepsilon = 0$ trivially, and one deals with classical probabilities instead of quantum behavior. Thus, a nonzero δ ensures that we are in a quantum mechanical regime. In an experiment, we never measure probabilities directly, but only absolute frequencies of photon occurrences. The quantity κ is independent of the total particle flux onto the slits as long as it is constant in time.

To measure κ in various optical power regimes, we used different types of photon sources. Figure 2 shows details of the experimental setup. We used a laser attenuated to a power level of a few microwatts down to ~200 fW (single-photon level) as well as heralded single photons (~40,000 photons/s) created by spontaneous parametric downconversion (5).
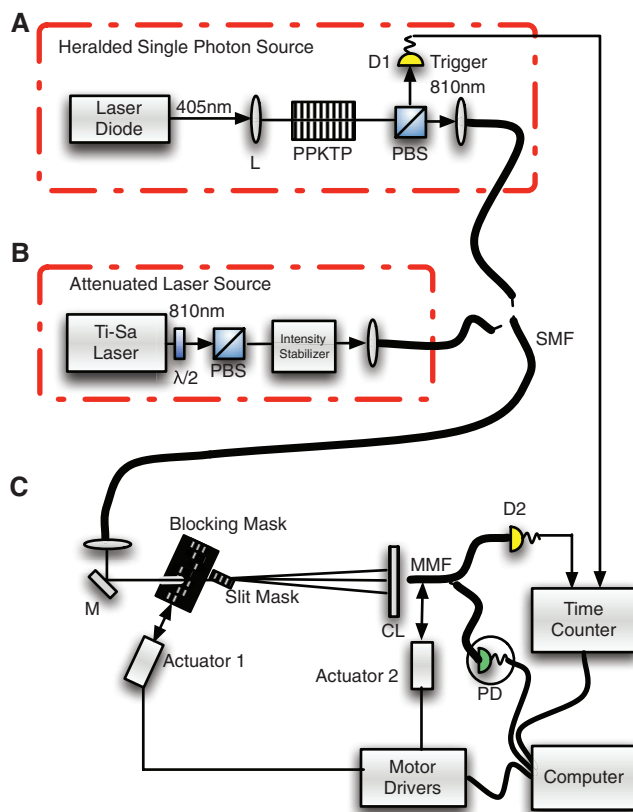
At the photon-counting level, the detection mechanism is based on a silicon avalanche photodiode (APD), and thus the particle-like nature of light is incorporated in the experiments. At the microwatt level, a series of measurements was performed with a standard optical power meter, using a silicon photodiode. The power meter measurements investigated the optical regime in which particle character is not of concern. In all cases we performed a large number of measurements at fixed points in the diffraction pattern [fig. S1 in (5)]. In addition, we have also performed measurements to check the variation of κ as a function of detector position. Born's rule would predict that κ should be independent of detector position. However, systematic errors may vary with the position and therefore are seen to bring a variation in the measured value of κ at different detector positions even in our experiment. Nonetheless, the mean κ is within the bounds set by the attendant errors at each such detector position.

The typical distributions of measured values of κ are shown in Fig. 3, with photon streams from a laser attenuated to different levels (Fig. 3, A and B) and from a heralded single-photon source (Fig. 3C). κ is calculated from the measured interference intensities for the eight independent slit combinations at a fixed position.

The order of the eight slit combinations was chosen randomly for reducing systematic influences on κ caused by slow variations of the photon flux. Each combination in a run was measured for a certain photon-count integration time, and up to 100 runs were cycled to obtain a statistically significant sample of κ values. Among the many positions in the diffraction pattern, we chose the central maximum of the triple-slit combination (yielding the maximum number of coincidence photon counts) to obtain our data (5). For the single-photon source, we measured at each slit combination until the trigger count reached 30 million, which was a good compromise between accumulating a statistically significant number of coincidences for the different slit combinations and ensuring a low drift of the photon source between measurements.

With a null experiment, a very careful analysis of random and systematic errors must be undertaken, as our bound on the amount of three-path interference will be directly related to the level of experimental uncertainty. Among the random errors in our setup, thermal and acoustic fluctuations cause the source fluxes to vary in time. In addition, detection efficiency and optical alignment can change. In particular, there will be some mechanical vibration of the thin (25 μm) slotted steel membrane apertures, causing a variable slit transmission due to near-field diffraction. In addition, for power meter measurements, the instrumental error is added to the above error sources, whereas for photon counting, the Poissonian distributed counting error is the dominating fluctuation. Because of the random nature of the individual errors, we used Gaussian error propagation to estimate the error of κ, where we used the standard variances of the individual measurement values calculated from a large number of repetitions of the experiments. In some cases where we observed a drift in the rates, we found the Allen variance of the values to be a better estimator for error propagation. This is justifiable because κ is calculated from eight measurements taken in direct succession, and the variance between subsequent samples of each quantity p_A, p_B, etc., is therefore the most suitable error estimator.

Once we understand the random errors, we can characterize the systematic errors. Our experiment and the measurement of κ are convenient, as they neither require the slits to be identical nor require the transmission values to be perfectly 1 and 0. On the other hand, what matters is the absence of correlation or systematic variation in how the slits behave while switching between slit combinations. Note that the size of the slits and the wavelength make independent shutters difficult to insert, and we used a static opening mask plate in front of the actual slits for blocking and unblocking the individual slits.

Our approach can potentially introduce unwanted correlations between the switching of different combinations. This occurred in our case; a fault in the blocking mask in the BC combination caused opening B to be shifted off its nominal

Fig. 2. Experimental set-up used for the measurement of κ. (**A**) Creation of heralded single photons from a periodically poled potassium titanyl phosphate (PPKTP) nonlinear crystal pumped by a 405-nm laser diode. Parametric downconverted photons are emitted as pairs at 810 nm and are coupled into a single-mode fiber (SMF). Photon detection (D1) in the trigger output heralds a single photon, which is then sent through the diffraction slits. (**B**) A pulsed titanium-sapphire (Ti-Sa) laser is attenuated and coupled into a SMF. The attenuation is realized by the combination of a half-wave plate (λ/2) and a polarizing beamsplitter (PBS), combined with neutral filters and an intensity stabilizer. (**C**) Schematic of the three-slit experiment where the photons from the source go through the movable blocking mask with the eight combinations and then through the slit mask, which has the three slits cut into it. We keep the slit mask stationary, whereas the blocking mask consists of bigger and wider slits that open up the various slit combinations as it moves up and down. In this way, we ensure that the same set of slits is used for measuring the different combinations, thus eliminating any dependence on the slit properties. The diffracted light is condensed vertically with a cylindrical lens (CL) onto a multimode fiber (MMF, core size 62.5 μm), ~180 mm from the slits. This fiber (movable along the diffraction pattern) acts as an aperture to probe the interferences. The collected photons are detected either with an avalanche photodiode (D2) whose signals are recorded with a time counter, or with an optical power meter (PD), both connected to a computer. For heralded single photons, detections are conditioned on the detection of a trigger photon.

position by 8 μm. At zero distance between opening and slit masks, this shift would not affect the transmittance of the diffracting slit. However, with the finite separation of 50 μm between the two masks, it does matter. Using a two-dimensional finite-difference time domain simulation of the light field between the wider opening and narrower slit, we found that this lateral misalignment could change the effective slit transmission by ±3%, depending on the relative position. Using this to adjust the slit transmittance value for slit *B* in the combination *BC* leads to a value of $|\kappa|$ = 0.01. Bringing the masks closer would reduce this error, but the thin membranes tend to stick together when they come closer than 50 μm.

Another major systematic error is detector nonlinearity. There is no perfect detector, and efficiency and nonlinearity will always be finite. For our commercial power meter, the nonlinearity is 0.5% for all ranges. For the worst case, at the central maximum of the diffraction pattern, this results in a systematic error of $|\kappa|$ = 0.003. For photon-counting detectors, there is always a finite dead-time during which they are blind to photons. Depending on the flux, this results in a saturation effect; that is, the detector response does not follow the square law, but has a deviation potentially indistinguishable from a violation of Born's rule. Therefore, to keep the nonlinearity error negligible, we used count rates below 100,000/s.

Combining the various error sources, our particular setup enables us to bound the measurements of κ to better than 0.01, thus providing a bound on the accuracy of Born's rule. This is in good agreement with the values measured for single photons, $\kappa = 0.0064 \pm 0.0120$, and for the attenuated laser beams, $\kappa = 0.0073 \pm 0.0018$ (power meter measurement) and $\kappa = 0.0034 \pm 0.0038$ (APD measurement) from Fig. 3.

Note that any significant nonzero observation of I_{ABC} would imply that Born's rule does not strictly hold. The consequences of detecting even

a small amount of three-way interference (by deviating from the quantum mechanical null prediction) would be tremendous. A modification to Born's rule that leads to multi-order interference would have repercussions on the allowable dynamics. In particular, if probability must be conserved, then Schrödinger's equation would likely have to be modified as well. Nonlinear extensions to quantum mechanics are one way to generalize it (*6*–*8*), and there have been efforts to test these nonlinearities (*9*–*12*). However, in such experiments, a model was assumed for the nonlinear variant of the Schrödinger equation, and efforts were concentrated on estimating the coefficient of the nonlinearity. In contrast, we present a dedicated test for Born's rule and are able to confirm it within our experimental limitations without depending on specific nonlinear extensions of quantum mechanics.

We are able to bound the magnitude of the third-order interference term to less than 10^{-2} of the regular expected second-order interference, at several detector positions. Thus, our experiment is able to rule out the existence of third-order interference terms (and, in effect, any higher-order interference terms) up to this bound. This bound on the accuracy of Born's rule is relevant for theoretical attempts to derive it (*13*) as well as for the generalization of quantum mechanics. Among the consequences of such a generalized theory, it would require more detailed specifications of the quantum system (*14*) and could modify computational complexity by allowing one to distinguish between orthogonal states, thus breaking quantum cryptography and making quantum computing more powerful [i.e., super-quantum computing (*15*)]. The triple-slit experiment is a simple and very natural system to investigate three-path interference, but it is not the only possible implementation; any configuration of three mutually exclusive quantum paths can be used in such a test. Although our implementation did not lead to the observation of any deviations, such future tests with other systems might indeed lead to improved accuracies on the bound of κ. It would be interesting to perform tests with other types of particles such as neutrons (*16*, *17*), tests of C_{60} molecule interference (*18*) or electron interference with slits or potential wells (*19*, *20*), or tests of a system with a global wave function, such as a Bose-Einstein condensate (*21*, *22*).
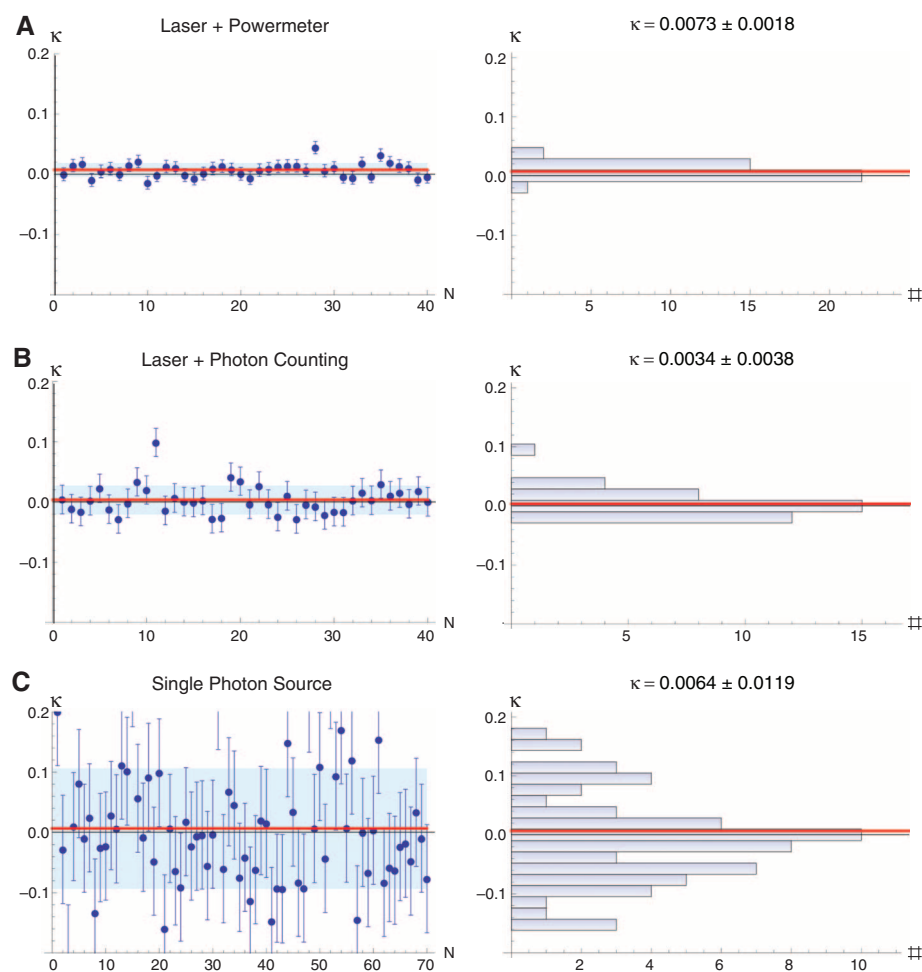
Fig. 3. Typical distributions of κ measured at the central maximum of the triple-slit interference pattern. (**A**) Data using a laser source and a power meter for detection, resulting in κ = 0.0073 ± 0.0018. (**B**) Data with the laser but attenuated to single-photon level and an APD for detection, resulting in κ = 0.0034 ±0.0038. (**C**) Data taken using the heralded single-photon source and an APD for detection, resulting in κ = 0.0064 ± 0.0119. The Allen variance of κ was used to plot the error bars. The horizontal red lines represent the mean κ values; the blue shaded regions represent a band of one standard deviation of the distribution of κ values around the mean.

References and Notes
1. M. Born, *Z. Phys.* **37**, 863 (1926).
2. R. D. Sorkin, *Mod. Phys. Lett. A* **9**, 3119 (1994).
3. P. Grangier, G. Roger, A. Aspect, *Europhys. Lett.* **1**, 173 (1986).
4. V. Jacques *et al.*, *Eur. Phys. J. D* **35**, 561 (2005).
5. See supporting material on *Science* Online.
6. S. Weinberg, *Phys. Rev. Lett.* **62**, 485 (1989).
7. I. Bialynicki-Birula, J. Mycielski, *Ann. Phys.* **100**, 62 (1976).
8. C. Simon, V. Buzek, N. Gisin, *Phys. Rev. Lett.* **87**, 170405 (2001).
9. R. Gähler, A. G. Klein, A. Zeilinger, *Phys. Rev. A* **23**, 1611 (1981).
10. J. J. Bollinger, J. D. Prestage, W. M. Itano, D. J. Wineland, *Phys. Rev. Lett.* **54**, 1000 (1985).

11. R. L. Walsworth, I. F. Silvera, E. M. Mattison, R. F. Vessot, *Phys. Rev. Lett.* **64**, 2599 (1990).
12. P. K. Majumder, B. J. Venema, S. K. Lamoreaux, B. R. Heckel, E. N. Fortson, *Phys. Rev. Lett.* **65**, 2931 (1990).
13. W. H. Zurek, *Phys. Rev. Lett.* **90**, 120404 (2003).
14. C. Ududec, H. Barnum, J. Emerson, *Found. Phys.* (2010).
15. S. Aaronson, *Proc. R. Soc. Lond. A* **461**, 3473 (2005).
16. J. Summhammer, H. Rauch, D. Tuppinger, *Phys. Rev. A* **36**, 4447 (1987).
17. A. Zeilinger, R. Gähler, C. Shull, W. Treimer, W. Mampe, *Rev. Mod. Phys.* **60**, 1067 (1988).
18. M. Arndt *et al.*, *Nature* **401**, 680 (1999).
19. A. Ohshita, N. Takayama, H. Tomita, *J. Electron. Microsc.* **34**, 357 (1985).
20. L. Gaudreau *et al.*, *Phys. Rev. Lett.* **97**, 036807 (2006).
21. M. R. Andrews *et al.*, *Science* **275**, 637 (1997).
22. M. Greiner, O. Mandel, T. W. Hänsch, I. Bloch, *Nature* **419**, 51 (2002).
23. U.S., C.C., and T.J. performed the experiments; C.C., R.L., and G.W. conceived of and supervised the experiment and developed the theoretical aspects; G.W. and U.S. performed the modeling and the data and error analysis; and all authors contributed to the writing of the paper. We thank H. Hübel, R. Kaltenbäck, A. J. Leggett, A. Sinha, R. D. Sorkin, and A. Zeilinger for valuable

Identification of Carbonate-Rich Outcrops on Mars by the Spirit Rover

Richard V. Morris,[1]* Steven W. Ruff,[2] Ralf Gellert,[3] Douglas W. Ming,[1] Raymond E. Arvidson,[4] Benton C. Clark,[5] D. C. Golden,[6] Kirsten Siebach,[4] Göstar Klingelhöfer,[7] Christian Schröder,[8] Iris Fleischer,[7] Albert S. Yen,[9] Steven W. Squyres[10]

Decades of speculation about a warmer, wetter Mars climate in the planet's first billion years postulate a denser CO_2-rich atmosphere than at present. Such an atmosphere should have led to the formation of outcrops rich in carbonate minerals, for which evidence has been sparse. Using the Mars Exploration Rover Spirit, we have now identified outcrops rich in magnesium-iron carbonate (16 to 34 weight percent) in the Columbia Hills of Gusev crater. Its composition approximates the average composition of the carbonate globules in martian meteorite ALH 84001. The Gusev carbonate probably precipitated from carbonate-bearing solutions under hydrothermal conditions at near-neutral pH in association with volcanic activity during the Noachian era.

The existence of carbonate minerals on Mars has long been postulated, based on evidence of past and present water along with a CO_2-rich atmosphere that may have been denser during the Noachian era (*1–5*). Carbonate minerals have been identified in martian meteorites as minor phases (~1 volume % or less) by petrographic and microbeam methods (*5*) and detected by orbital observations in regional-scale rock units in Nili Fossae at unknown abundances (*6*) and, equivocally, in martian dust and in soil as a minor component (<5 volume %) (*7–10*). Here, we describe the detection of carbonate as a major component in outcrops in the Columbia Hills of Gusev crater.

The Columbia Hills are an "island" of older rocks surrounded by Hesperian-aged olivine-bearing volcanic rocks that dominate the plains within Gusev crater (*11*). The Hills form a crudely antiformal structure composed of massive-to-layered rocks with varying compositions and extents of aqueous alteration (*12–16*). The Inner Basin within the Hills is dominated by volcaniclastic rocks, including Home Plate, and alteration phases (sulfates and opaline silica deposits) of likely hydrothermal origin (*17–21*). The Mars Exploration Rover Spirit descended from Haskin Ridge on the eastern side of the summit of Husband Hill into the Inner Basin of the Columbia Hills to the eastern edge of the El Dorado ripple field during its second summer at Gusev crater (*16*). A series of benches (Fig. 1) with olivine-rich outcrops were encountered and analyzed by Spirit's instruments (*19, 21*). The Comanche outcrops, with their granular surface textures (grain sizes ~0.5 to 1.0 mm), are erosional remnants that are draped over the older and more massive Algonquin and other olivine- and pyroxene-rich outcrops (Figs. 1 and 2). They have layering whose bedding is roughly conformal with local topography, consistent with a volcaniclastic origin, and have fracture-filling deposits that have withstood aeolian erosion better than the surrounding materials, forming raised fins (Figs. 1 and 2).

Spirit's Mössbauer (MB) spectrometer provides information about Fe mineralogy and the distribution of Fe among Fe-bearing phases and oxidation states (*22*). The MB spectrum of Comanche Spur (Fig. 3A) is characterized by two Fe^{2+} doublets, which were initially assigned to Fe^{2+} in olivine and to either Fe^{2+} in pyroxene atypical of other Gusev pyroxenes or to Fe^{2+} in a phase other than pyroxene (*19*). The doublet identification diagram (Fig. 3B), which now includes data for Fe^{2+}-bearing carbonates (*23*), shows that

Comanche Spur is an olivine-carbonate assemblage. The MB data indicate the presence of Mg-Fe carbonate in the Comanche outcrops [Fig. 3B and (*23*)].

In addition to major element chemistry, the Spirit's Alpha Particle X-Ray Spectrometer (APXS) instrument can determine an aggregate concentration for excess light elements through analysis of photon scattering peaks (*24, 25*). The energy of the APXS scattering photons (14.3 keV) is virtually identical to that for the MB gamma ray (14.4 keV), so that the depth of rock analyzed by the two instruments is equivalent. The average excess light-element concentration of Comanche Spur, measured on surfaces brushed by the Rock Abrasion Tool (RAT), is 12 ± 5 weight percent (wt %) equivalent CO_2 (Table 1). The low bulk CaO concentration of Comanche Spur (1.69 wt %) requires that the carbonate have a low Ca content, consistent with MB data (Fig. 3B). For comparison, the excess light-element concentration of Algonquin is 0 ± 5 wt % equivalent CO_2. The carbonate content of Comanche is equivalent to ~3% C in the sample. Because of CO_2 in the martian atmosphere, this value is close to the expected APXS alpha channel detection limit for C, so we have not been able to use alpha data to detect C specifically.

We calculated the chemical composition of Comanche carbonate and olivine using previously reported APXS data (*21*), recalculated to include CO_2, and the percentages of Fe associated with those phases from MB data (Fig. 3A). The calculations yielded (Table 1) a Mg-Fe carbonate ($Mc_{0.62}Sd_{0.25}Cc_{0.11}Rh_{0.02}$, where Mc = magnesite, Sd = siderite, Cc = calcite, and Rh = rhodochrosite) and a forsteritic olivine ($Fo_{0.72}Fa_{0.28}$, where Fo = forsterite and Fa = fayalite). All Ca and Mn was assigned to the carbonate to give an upper-limit concentration for those elements, but we have no information as to their actual phase association. The calculated carbonate and olivine compositions are $Mc_{0.75}Sd_{0.25}$ and $Fo_{0.70}Fa_{0.30}$ when Ca and Mn are not associated with the carbonate. In either case, the concentration of carbonate in Comanche Spur is ~26 wt % (Table 1). Using the 7.0 to 17.0 wt % range of the CO_2 concentration (Table 1), the range in the carbonate concentration is ~16 to 34 wt %.

Spectra obtained by Spirit's Miniature Thermal Emission Spectrometer (Mini-TES) provide

[1]NASA Johnson Space Center, Houston, TX 77058, USA. [2]Arizona State University, Tempe, AZ 85287, USA. [3]University of Guelph, Guelph, Ontario, Canada. [4]Washington University in Saint Louis, St. Louis, MO 63130, USA. [5]Space Sciences Institute, Boulder, CO 80301, USA. [6]Engineering and Science Contract Group–Hamilton Sundstrand, Houston, TX 77058, USA. [7]Johannes Gutenberg-Universität, Mainz, Germany. [8]University of Bayreuth and Eberhard Karls University of Tübingen, Tübingen, Germany. [9]Jet Propulsion Laboratory, Pasadena, CA 91109, USA. [10]Cornell University, Ithaca, NY 14853, USA.

*To whom correspondence should be addressed. E-mail: richard.v.morris@nasa.gov